Role of Interchain Coupling in the Metallic State of Conducting Polymers

Nara Kim,[1] Byoung Hoon Lee,[1] Doowhan Choi,[2] Geunjin Kim,[1] Heejoo Kim,[3] Jae-Ryoung Kim,[3] Jongjin Lee,[3] Yung Ho Kahng,[3,*] and Kwanghee Lee[1,2,3,†]

[1]*School of Materials Science and Engineering, Gwangju Institute of Science and Technology, Gwangju 500-712, Korea*
[2]*Department of Photonics and Applied Physics, Gwangju Institute of Science and Technology, Gwangju 500-712, Korea*
[3]*Research Institute for Solar and Sustainable Energies, Gwangju Institute of Science and Technology, Gwangju 500-712, Korea*

(Received 27 April 2012; published 7 September 2012)

We investigated the charge dynamics of the conductivity enhancement from 2 to 1000 S/cm in poly(3, 4-ethylenedioxythiophene):poly(styrenesulfonate) as induced by structural changes through the addition of a polar solvent and the following solvent bath treatment. Our results indicate that the addition of a polar solvent selectively enhanced the π-π coupling of the polymer chains, resulting in the reduction of disorder and tremendously increasing the charge carrier mobility, which yielded an insulator-to-metal transition. In contrast, the following solvent bath treatment selectively enhanced the intergrain coupling, which did not affect the disorder or the mobility but increased the charge carrier density. Therefore, we demonstrate that the conduction-character defining disorder in this conducting polymer system is determined by the extent of interchain coupling.

DOI: 10.1103/PhysRevLett.109.106405 PACS numbers: 71.30.+h, 72.80.Le, 81.40.Rs

The discovery of conducting polymers in 1977 created an interdisciplinary research field between chemistry and condensed-matter physics [1]. The electrical conduction is known to arise from the charge carriers induced by chemical doping and the mobility of the charge carriers along π-conjugated polymer chains [2]. However, the nature of the charge dynamics in conducting polymers is not yet fully understood. While the charge dynamics in conventional metals is well described by the Drude model [3], in noncrystalline conducting polymers formed by the uncontrolled packing of 1D polymer chains the charge carriers are localized by disorder and are typically transferred by phonon-assisted hopping [4]. However, with the recent progress in the synthesis and processing of conducting polymers, which has improved their ordering and conductivity (σ_{dc}), the charge dynamics in many of these polymers deviates from the hopping model [5,6]. Therefore, the need for a new description of the charge dynamics for highly conducting polymers has emerged, though progress in developing this model has been slow.

One of the main issues is that the effective length scale of the disorder has been debated considerably, pitting the ''homogeneous model'' versus the ''inhomogeneous model'' [6–9]. In the homogeneous model, the ''interchain coupling'' among nanoscale 1D conducting polymer chains is considered to be critical for the 3D conduction [7–9]. In contrast, in the inhomogeneous model, the ''intergrain coupling'' among microscale high-conducting crystalline grains embedded in low-conducting amorphous media is considered to be more important [5–8]. However, earlier studies on the nature of the charge dynamics in conducting polymers adopted control parameters involving external stimuli, such as pressure and/or magnetic field or different synthesis processes, which could not selectively change the interchain or intergrain coupling. Therefore, the results were ambiguous and could not be used to settle the debate about the two conducting models [7–9].

Poly(3, 4-ethylenedioxythiophene):poly(styrenesulfonate) (PEDOT:PSS), in which PSS acts as both a soluble template and a charge-balancing counterion for PEDOT, consists of hydrophobic, conductive, PEDOT-rich grains embedded in a hydrophilic, insulating, PSS-rich matrix and thus is a model system for the granular conducting polymers [10]. In particular, highly conducting states of PEDOT:PSS have been induced by the addition and/or the bath treatment of a polar solvent, such as dimethyl sulfoxide (DMSO), ethylene glycol (EG), sorbitol, or glycerol, into the PEDOT:PSS aqueous solution, increasing the σ_{dc} by 2–3 orders of magnitude [11–13]. However, the physics behind such an impressive σ_{dc} increase has not been clearly explained [14]. Studies have suggested that the mechanism is due to polymer chain expansions [11] or due to the phase separation between the conducting PEDOT-rich grains and the insulating PSS [12].

In this Letter, we investigated the charge dynamics of a 500-fold conductivity enhancement in PEDOT:PSS as induced by structural changes through the addition of DMSO and the additional EG-bath treatment by measuring the x-ray diffraction (XRD), the temperature (T)-dependent σ_{dc}, and the reflectance spectra [$R(\omega)$]. Our results indicate that the addition of DMSO selectively enhanced the π-π ''interchain coupling'' of the conducting PEDOTs through the increased interchain packing, resulting in significant enhancement in σ_{dc} from 2 to 700 S/cm at 295 K. A significant reduction of disorder and a huge increase in the charge carrier mobility (μ) were induced by adding DMSO to PEDOT:PSS, which yielded an insulator-to-metal (I-M) transition. In contrast, the additional EG-bath treatment selectively enhanced the ''intergrain

coupling'' by removing the PSS content in the insulating PSS matrix. The extent of disorder and μ were retained after the bath treatment, but the charge carrier density was increased, resulting in $\sigma_{dc} \approx 1000$ S/cm at 295 K. Therefore, our results unambiguously indicate that the homogeneous model is the governing conduction mechanism in this conducting polymer system.

PEDOT:PSS aqueous solutions (Clevios PH1000) were purchased from H. C. Starck. Solutions with or without 5 wt % DMSO were drop cast on glass or Si substrates to form PEDOT:PSS films with thicknesses of 60 μm to 80 μm. For an additional solvent treatment, some of the DMSO-treated samples were then immersed in an EG bath for 15 h at room temperature (RT). The XRD patterns were obtained using a Rigaku D/max-2500 diffractometer in a conventional θ-2θ geometry, with Cu-$K\alpha$ radiation ($\lambda = 1.540593$ Å) at 40 kV and 100 mA. The work functions were measured using a KP 6500 Digital Kelvin Probe (McAllister Technical Services. Co. Ltd.). For the T-dependent σ_{dc} measurements over the T range from 5 K to 295 K, both the four-lead and Van der Pauw methods [15] were used in a continuous-flow He cryostat. The $R(\omega)$ spectra were measured over the spectral range of 0.01 eV to 6.1 eV at RT using a Bruker Vertex 70 FT-IR spectrometer (0.01–1 eV) and a Perkin-Elmer Lambda 750 UV/Vis/NIR spectrophotometer (0.5–6.1 eV). The optical conductivity spectra [$\sigma(\omega)$] were calculated by the Kramers-Kronig (K-K) transformation of $R(\omega)$ with proper extrapolations, as discussed earlier [16].

Figure 1(a) shows the XRD patterns obtained from the three different types of PEDOT:PSS samples prepared with various solvent treatments: the PEDOT:PSS sample without solvent treatment (denoted as pristine), the PEDOT:PSS sample treated with DMSO (denoted as DMSO-P), and the DMSO-P sample with an additional EG-bath treatment (denoted as EG DMSO-P). The six distinct peaks at 2θ values of approximately 3.8°, 6.7°, 10°, 13.8°, 17.7°, and 26° correspond to lattice spacings of approximately 23, 13.2, 8.8, 6.4, 5.0, and 3.4 Å, respectively, as calculated using Bragg's law [17]. The long-distance (23 Å) peak observed at 3.8° can be attributed to the alternate ordering distance of the PEDOT and PSS chains in the plane, that is, the lamella stacking distance [$d_{(100)}$], because the widths of the PEDOT and PSS chains are 7.5 and 15.5 Å, respectively, based on their chemical structures [18]. The spacing of 3.4 Å calculated from the peak at 26° is known to be the π-π stacking distance [$d_{(010)}$] of the aromatic rings of PEDOT [19]. However, the identities of the other peaks are less clear; our presumptions about the identities of the other peaks are as follows: the peak at 6.7° represents the interdigitation packing distance for PSS, and the peak at 17.7° represents the π-π stacking distance for PSS.

Interestingly, there is a clear difference in the two peaks at 3.8° and 26° of the PEDOT:PSS samples with and without the DMSO treatment; with the DMSO treatment, the $d_{(100)}$ peak shifted to a lower angle, while the $d_{(010)}$ peak

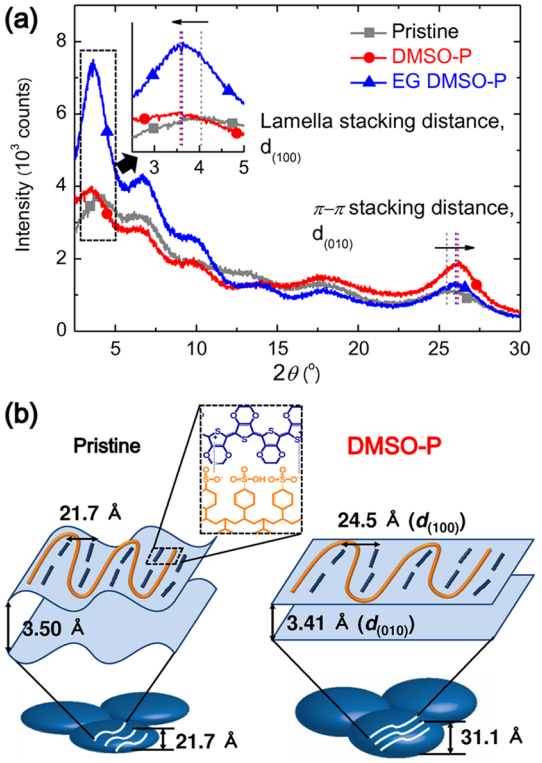

FIG. 1 (color online). (a) X-ray diffractograms measured from the three types of PEDOT:PSS samples. (b) Schematic diagrams showing the structural change of the PEDOT:PSS by the polar solvent addition as inferred from the x-ray data. The stacking distances ($d_{(100)}$ and $d_{(010)}$) and crystalline domain sizes of the $d_{(010)}$ stacking are indicated in the figure.

shifted to a higher angle, implying an increase in $d_{(100)}$ and a decrease in $d_{(010)}$, respectively. In addition, both peaks became larger and sharper, indicating that the crystalline domains grew in terms of number and thickness. The stacking distances calculated using Bragg's law and the vertical crystalline domain sizes of the $d_{(010)}$ stacking calculated from the Scherrer formula [17] are indicated in the schematic diagram presented in Fig. 1(b). As shown in the diagram, the changes of the distances $d_{(100)}$ and $d_{(010)}$ indicate that the layers consisting of alternating PEDOT and PSS polymer chains became more planar with the DMSO treatment, and consequently, the interlayer stacking distance of the PEDOTs decreased. It is well known that a decrease in $d_{(010)}$ corresponds to an increase in the degree of molecular packing and thus to an increase in the local crystallinity, as revealed by the peak sharpening and the surface roughening (see the Supplemental Material [20]) [21]. Based on our observation, we can conclude that the π-π interchain coupling of conducting PEDOTs in the PEDOT:PSS film was improved with the DMSO treatment because the interchain distance and local ordering of polymer chains exponentially affect the π-electronic overlap, which provides a pathway for π-π interchain charge transfer over an individual polymer [22]. In this case, the intergrain coupling did not increase significantly because the

same amount of insulating PSS matrix remained in the PEDOT:PSS films with and without DMSO treatment and the lateral grain diameter increased slightly from 52 to 55 nm (Table S1) [6].

For the EG DMSO-P sample, $d_{(100)}$ and $d_{(010)}$ were the same as those in the DMSO-P sample, indicating a similar level of interchain coupling. Meanwhile, there were changes in the peak intensities; the long-periodicity peaks, such as $d_{(100)}$, increased, while the short-periodicity peaks, such as $d_{(010)}$, decreased. These changes imply a shift in the orientation of the PEDOT:PSS layers from the horizontal direction to a more perpendicular direction with respect to the substrate with the EG-bath treatment because in a θ-2θ geometry, only the lattice orders parallel to the substrate can be detected. These structural changes are induced by the selective removal of the excess PSS in the PEDOT:PSS films by the additional EG-bath treatment, as evidenced by the decrease in the peaks from PSS alone in the absorption spectra of PEDOT:PSS in a previous report [13] and the decrease in the work function of the PEDOT:PSS samples from 5.2 to 5.0 eV in our experiment [23]. After the bath treatment, we found that the thickness of the film decreased by as much as 30%, indicating that a large amount of PSS in the insulating matrix is removed, and therefore, a significant increase of the intergrain coupling between the PEDOT-rich grains can be assumed to have occurred.

Figure 2(a) plots the $\sigma_{dc}(T)$ values of three different types of PEDOT:PSS samples. For the pristine sample, $\sigma_{dc}(T)$ increased rapidly to a maximum of approximately 2 S/cm as T increased from 5.5 K to RT. This strong T dependence and the extrapolation to zero conductivity at 0 K are characteristics of typical insulators. In addition, the large ratio of the resistivities, $\rho(5.5\ \mathrm{K})/\rho(295\ \mathrm{K}) > 6000$, indicates a high level of disorder in this sample [9,24]. In contrast, the DMSO-P sample exhibited a weak T dependence and a 350-fold increased maximum σ_{dc} at RT. Further enhancement of σ_{dc} up to 1000 S/cm was induced in the EG DMSO-P sample. The σ_{dc} values for both the DMSO-P and EG DMSO-P samples can be extrapolated to a finite value above 200 S/cm as T approaches 0 K. This behavior is characteristic of metallic conduction. The reduced activation energy, $W = (\Delta \ln\sigma_{dc}/\Delta \ln T)$ vs T, in the inset of Fig. 2(a) demonstrates the crossover of the slopes from a negative value (pristine) to positive values (DMSO-P and EG DMSO-P) at low T, which clearly reveals that the solvent treatments induced an I-M transition in our samples [25].

Furthermore, we compared our $\sigma_{dc}(T)$ data with those obtained via various conduction models. Figures 2(b) and 2(c) present the fitting results. For the pristine sample, the data were well-fitted to the quasi-2D variable-range hopping (VRH) model: $\sigma_{dc}(T) = \sigma_0 \exp[-(T_0/T)^{1/1+x}]$, where σ_0 is the conductivity at infinite T, T_0 is the characteristic temperature, and x is the dimensionality of the system [26]. The fit to the pristine sample yielded $x = 1.74$ and $T_0 = 4365$ K for the entire T range [Fig. 2(b)], while the other samples did not display any good fits [Fig. 2(b), inset]. These results indicate that the charge transport in the pristine sample can be attributed to the phonon-assisted hopping between quasi-2D localized states.

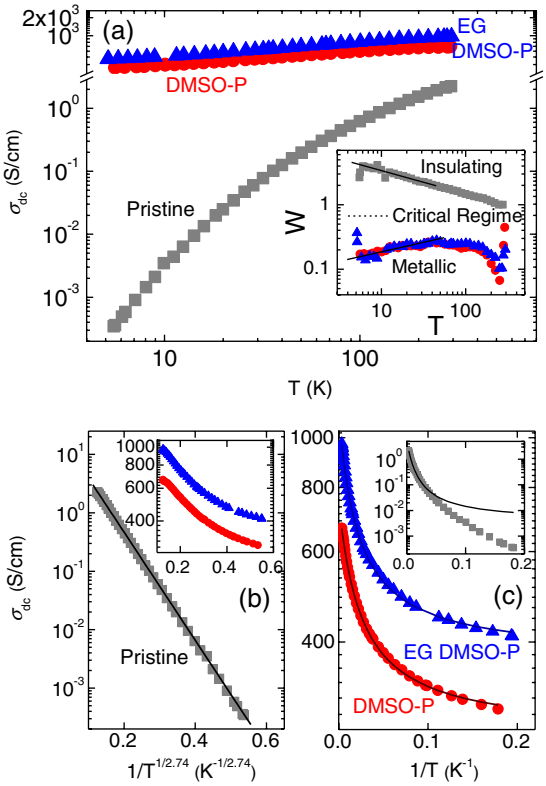

FIG. 2 (color online). (a) T dependence of σ_{dc} for the three types of PEDOT:PSS samples. The inset plots the reduced activation energy, $W = (\Delta \ln\sigma_{dc}/\Delta \ln T)$. (b) Log of σ_{dc} vs $(1/T)^{1/2.74}$ plot for the pristine sample data. The straight line indicates that the quasi-2D (1.74D) VRH model is suitable to describe the data. (c) Log of σ_{dc} vs $1/T$ plots for the solvent-treated samples. The solid curves are calculated from the FIT model. The insets in (b) and (c) present the fit results for the other samples.

However, the $\sigma_{dc}(T)$ data of the solvent-treated PEDOT:PSS samples were well-fitted to the fluctuation-induced tunneling (FIT) model [Fig. 2(c)], which represents tunneling through plane-parallel junctions of the barrier potential V_0, area A, and width w: $\sigma_{dc}(T) = \sigma_0 \exp(-\frac{T_1}{T+T_0})$, where $T_1 = 2AV_0^2/\pi e^2 k_B w$ and $T_0 = T_1(2\hbar^2/\pi^2 m^* V_0 w^2)^{1/2}$. k_B is the Boltzmann constant, m^* is the effective mass of the charge carrier, and $\hbar$ is the reduced Planck constant [27]. The pristine sample did not yield a good fit [Fig. 2(c), inset]. As apparent in the equation, the FIT model yields a finite $\sigma_{dc}(0)$. The fits to the DMSO-P and EG DMSO-P samples yielded $T_1 = 38.3$ K and $T_0 = 40.1$ K and $T_1 = 45.0$ K and $T_0 = 49.6$ K, respectively. The T_1 and T_0 values from the solvent-treated PEDOT:PSS samples are

comparable to those obtained from the highly conducting polyacetylene samples in earlier reports [28].

The change in the conduction model that fits the $\sigma_{dc}(T)$ data from the quasi-2D VRH to the FIT through the plane-parallel junctions with the DMSO treatment confirms the increased π-π interchain coupling as revealed by the XRD results. In the pristine sample, the charge transport between sheets consisting of several intertwined PEDOT:PSS chains is suppressed by the absence of finite interchain coupling because of the corrugation in the sheets [29]. Thus, the macroscopic conductivity is dominated by hopping transport between the quasi-2D conducting sheets, yielding a localized insulating state in the macroscopic sample. However, in the DMSO-P sample, the interaction between the polar solvents and the PEDOT:PSS chains increases the planarity of the quasi-2D PEDOT:PSS sheets (perhaps by polymer chain expansion [11]). Thus, the increased packing of the sheets and the strong interchain coupling facilitate tunneling of the charge carriers between the sheets, consequently yielding a delocalized metallic state in the macroscopic sample. Meanwhile, a similar level of interchain coupling in the DMSO-P and the EG DMSO-P samples caused similar tunneling barriers.

Figure 3 plots the $R(\omega)$ values of the three types of PEDOT:PSS samples over a wide spectral range. In the infrared (IR) region, the metal-like signatures of PEDOT, such as the well-defined minimum at the plasma frequency (ω_P) and high $R(\omega)$ in the far-IR arising from the intraband transitions, were observed [30]. The two small peaks observed in the ultraviolet region (near 5 and 6 eV) are due to the interband transitions in PSS [31]. The corresponding $\sigma(\omega)$ values reveal the dynamics of the charge carriers [32]. The features of the peak centered at approximately 550 cm^{-1} and a decrease toward $\sigma_{dc}(RT)$ with decreasing ω result from the weak localization of the charge carriers induced by disorder [33]. The charge dynamics of weakly localized conductors can be quantitatively analyzed by the localization-modified Drude (LMD) model [16,33] as follows:

$$\sigma_{LD}(\omega) = \frac{{\omega_P}^2\tau}{4\pi(1+\omega^2\tau^2)}\left\{1-\frac{C}{(k_F l)^2}[1-(3\tau\omega)^{1/2}]\right\} = \sigma_{Drude}(\omega)\left\{1-\frac{C}{(k_F l)^2}[1-(3\tau\omega)^{1/2}]\right\},$$

where τ is the mean free time, $C \approx 1$, k_F is the Fermi wave number, and l is the mean free path. The parameter $k_F l$ characterizes the extent of disorder in localization theory

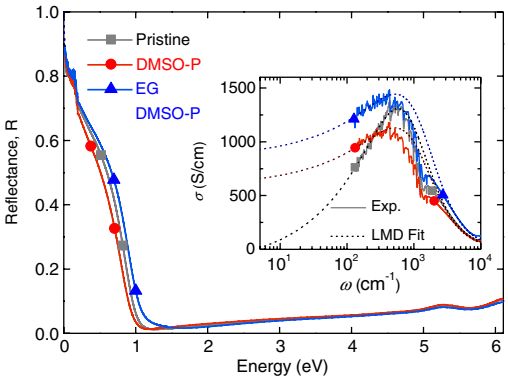

FIG. 3 (color online). $R(\omega)$ values of the three types of PEDOT:PSS samples. The inset shows the $\sigma(\omega)$ values obtained from the K-K analyses of $R(\omega)$ and the theoretical fits to the LMD model (dashed lines). 1 eV = 8065 cm^{-1}.

[34]. As presented in the inset of Fig. 3, the LMD model fits the $\sigma(\omega)$ values of each sample well, except for the IR-active vibrational (IRAV) modes observed at 400–2000 cm^{-1}. The parameters obtained from the fittings are listed in Table I. The $\sigma_{dc}(RT)$ values obtained independently from the dc transport measurements agreed with the $\sigma_{LD}(\omega \to 0)$ values within the error range, confirming the accuracy of the $R(\omega)$ measurements and the adequacy of the LMD model fits to the PEDOT:PSS sample data. In addition, the ω_P values were obtained from the LMD model fits and correspond well with the ω values at the $R(\omega)$ minima. Assuming that m^* is equal to the free electron mass, the n and μ values were calculated from ${\omega_P}^2 = 4\pi e^2 n/m^*$ and $\sigma_{dc} = ne\mu$, respectively, (Table I).

Upon the addition of DMSO, the ω dependence of $\sigma(\omega)$ in the far-IR region became weaker, and the conductance-maximum ω shifted to a lower value. Furthermore, as mentioned above, the extrapolated dc conductance value increased significantly. This change in $\sigma(\omega)$ is reflected in the increase of the order parameter, $k_F l$, from 0.96 (pristine) to 1.39 (DMSO-P), which crosses the Ioffe-Regel criterion, $k_F l \approx 1$, defining the point where disorder-induced I-M transition occurs [26,35]. Thus, the addition of DMSO induced an I-M transition with a huge increase in μ in the PEDOT:PSS sample. This observation corroborates our conclusion from the $\sigma_{dc}(T)$ measurements. Furthermore, it can be deduced that the I-M transition between the pristine and DMSO-P samples is mainly induced by the reduction in the material's disorder because ω_P and τ only change by an insignificant amount. Therefore, the comprehensive results from the structural,

TABLE I. The measured dc conductivities, parameters obtained from the LMD fits to $\sigma(\omega)$, and the calculated charge carrier concentration and mobility. Five samples were measured for each sample condition.

Sample	σ_{dc} (S/cm)	$\sigma_{LD}(0)$ (S/cm)	ω_P (eV)	τ (fs)	$k_F l$	n (10^{21}/cm^3)	μ (cm^2/V s)
Pristine	2.0 ± 0.9	-	1.09 ± 0.03	5.63 ± 0.20	0.96 ± 0.02	0.86 ± 0.05	0.015 ± 0.008
DMSO-P	660 ± 100	590 ± 90	1.19 ± 0.04	4.18 ± 0.11	1.39 ± 0.08	1.03 ± 0.07	4.0 ± 0.9
EG DMSO-P	960 ± 140	860 ± 120	1.44 ± 0.02	3.83 ± 0.12	1.44 ± 0.08	1.50 ± 0.04	4.0 ± 0.7

transport, and optical measurements confirm that the enhancement of interchain coupling is the major factor for the reduction of disorder and the manifestation of a metallic state in our conducting polymer system.

However, the increase in $\sigma(\omega)$ after an additional EG-bath treatment is due to the increase in the charge carrier concentration (n) by a factor of 1.5, which coincides with the increase in the average σ_{dc} of the DMSO-P sample compared with that of the EG DMSO-P sample. This increase in the n results from the reduced excess PSS by the EG-bath treatment, as mentioned above, whereas the extent of disorder remains similar, as indicated by the similar $k_F l$ and μ values shown in Table I. Therefore, it can be concluded that the enhancement of the intergrain coupling does not significantly facilitate the charge transport in the PEDOT:PSS, indicating that the homogeneous model describes the conduction mechanism well.

On the critical evaluation of our results, one could argue that the phase separation of the PEDOT-rich grains and the PSS-rich matrix occurred with the DMSO treatment [12], significantly thinning the intergrain boundaries. The additional EG-bath treatment removed only the phase-separated PSS contents. According to this scenario, the inhomogeneous model can still be thought to describe the conduction mechanism of our sample. However, we reject this conduction scenario because of the following observations. With the additional EG-bath treatment, the volume faction of conducting PEDOT-rich grains increased from 32% to 46%. According to a 3D percolation observation of globular conducting particles in an insulating matrix [36], such a volumetric increase of the conducting grains increased the μ twice because the conducting paths in the material increased. However, our μ values did not increase with the additional EG-bath treatment (Table I).

In summary, our results demonstrate that the conduction-character defining disorder in PEDOT:PSS is determined by the extent of interchain coupling of the PEDOT:PSS chains in the quasi-2D localized states in agreement with the homogeneous model. This work may contribute to the fundamental understanding of the conduction physics of conducting polymers and the development of a realistic strategy for improving the conduction of conducting polymers.

We would like to thank the Heeger Center for Advanced Materials (HCAM) and the Research Institute for Solar and Sustainable Energies (RISE) at the Gwangju Institute of Science and Technology (GIST) for their assistance with the measurements. This work was supported by a National Research Foundation of Korea (NRF) grant funded by the Korean government (MEST) (No. 20090093869). K. L. also acknowledges the support provided by the World-Class University Program funded by the Ministry of Education, Science and Technology through the NRF (R31-10026) and the Basic Science Research Program through the NRF funded by the Ministry of Education, Science and Technology (R15-2008-006-02001-0).

*yhkahng@gist.ac.kr
†klee@gist.ac.kr

[1] C. K. Chiang *et al.*, Phys. Rev. Lett. **39**, 1098 (1977).
[2] A. J. Heeger, Rev. Mod. Phys. **73**, 681 (2001).
[3] N. W. Ashcroft and N. D. Mermin, *Solid State Physics* (Saunders, Philadelphia, 1976).
[4] L. Zuppiroli *et al.*, Phys. Rev. B **50**, 5196 (1994).
[5] R. S. Kohlman *et al.*, Phys. Rev. Lett. **74**, 773 (1995).
[6] V. N. Prigodin and A. J. Epstein, Synth. Met. **125**, 43 (2002).
[7] R. S. Kohlman and A. J. Epstein, in *Handbook of Conducting Polymers* (Marcel Dekker, New York, 1998).
[8] A. J. Heeger, Phys. Scr. **T102**, 30 (2002).
[9] R. Menon *et al.*, in *Handbook of Conducting Polymers* (Marcel Dekker, New York, 1998).
[10] U. Lang *et al.*, Adv. Funct. Mater. **19**, 1215 (2009).
[11] J. Ouyang *et al.*, Polymer **45**, 8443 (2004).
[12] X. Crispin *et al.*, Chem. Mater. **18**, 4354 (2006).
[13] Y. H. Kim *et al.*, Adv. Funct. Mater. **21**, 1076 (2011).
[14] M. Vosgueritchian, D. J. Lipomi, and Z. Bao, Adv. Funct. Mater. **22**, 421 (2012).
[15] S. Roth and D. Carroll, *One-Dimensional Metals* (Wiley-VCH, Weinheim, 2004).
[16] K. Lee, A. J. Heeger, and Y. Cao, Phys. Rev. B **48**, 14884 (1993).
[17] B. D. Cullity, *Elements of X-Ray Diffraction* (Addison-Wesley, Reading, MA, 1956).
[18] A. Lenz *et al.*, Chem. Phys. **384**, 44 (2011).
[19] K. E. Aasmundtveit *et al.*, Synth. Met. **101**, 561 (1999).
[20] See Supplemental Material at http://link.aps.org/supplemental/10.1103/PhysRevLett.109.106405 for details about the surface morphology of the three types of PEODT:PSS samples (AFM images, rms surface roughnesses, and lateral grain diameters).
[21] Y.-H. Kim, H.-S. Kim, and S.-K. Kwon, Macromolecules **38**, 7950 (2005).
[22] H. C. F. Martens, H. B. Brom, and R. Menon, Phys. Rev. B **64**, 201102(R) (2001).
[23] T.-W. Lee and Y. Chung, Adv. Funct. Mater. **18**, 2246 (2008).
[24] A. S. Dhoot *et al.*, Phys. Rev. Lett. **96**, 246403 (2006).
[25] A. G. Zabrodskii and K. N. Zeninova, Zh. Eksp. Teor. Fiz. **86**, 727 (1984).
[26] N. F. Mott and E. A. Davis, *Electronic Processes in Non-Crystalline Materials* (Clarendon, Oxford, 1979).
[27] P. Sheng, E. K. Sichel, and J. I. Gittleman, Phys. Rev. Lett. **40**, 1197 (1978).
[28] Y.-W. Park *et al.*, J. Chem. Phys. **73**, 946 (1980).
[29] J. Yi and B. J. Kim, Phys. Rev. B **76**, 245207 (2007).
[30] K. Lee and A. J. Heeger, Phys. Rev. B **68**, 035201 (2003).
[31] L. A. A. Pettersson, S. Ghosh, and O. Inganäs, Org. Electron. **3**, 143 (2002).
[32] K. Lee, in *Encyclopedia of Nanoscience and Nanotechnology* (American Scientific Publishers, San Diego, 2004), Vol. 5.
[33] N. F. Mott and M. Kaveh, Adv. Phys. **34**, 329 (1985).
[34] P. A. Lee and T. V. Ramakrishnan, Rev. Mod. Phys. **57**, 287 (1985).
[35] A. F. Ioffe and A. R. Regel, Prog. Semicond. **4**, 237 (1960).
[36] S. Hotta, S. D. D. VRughooputh, and A. J. Heeger, Synth. Met. **22**, 79 (1987).